ARTICLE

Thermochemical Energy Storage Performance of Zinc Destabilized Calcium Hydride at High-Temperatures†

Received 00th January 20xx,
Accepted 00th January 20xx

DOI: 10.1039/x0xx00000x

Sruthy Balakrishnan,[a] M. Veronica Sofianos,[a,b*] Terry D. Humphries,[a] Mark Paskevicius,[a*] and Craig E. Buckley [a]

CaH_2 has 20 times the energy density of molten salts and was patented in 2010 as a potential solar thermal energy storage material. Unfortunately, its high operating temperature (> 1000 °C) and corrosivity at that temperature make it challenging to use as thermal energy storage (TES) material in concentrating solar power (CSP) plants. To overcome these practical limitations, here we propose, the thermodynamic destabilization of CaH_2 with Zn metal. It is a unique approach that reduces the decomposition temperature of pure CaH_2 (1100 °C at 1 bar of H_2 pressure) to 597 °C at 1 bar of H_2 pressure. Its new decomposition temperature is closer to the required target temperature range for TES materials used in proposed third-generation high-temperature CSP plants. A three-step dehydrogenation reaction between CaH_2 and Zn (1: 3 molar ratio) was identified from mass spectrometry, temperature-programmed desorption and *in-situ* X-ray diffraction studies. Three reaction products, $CaZn_{13}$, $CaZn_{11}$ and $CaZn_5$, were confirmed from *in-situ* X-ray diffraction studies at 190 °C, 390 °C and 590 °C, respectively. The experimental enthalpy and entropy of the second hydrogen release reaction were determined by pressure composition isotherm measurements, conducted between 565 and 614 °C, as ΔH_{des} = 131 ± 4 kJ.mol^{-1} H_2 and ΔS_{des} = 151 ± 4 J.K^{-1}mol^{-1} H_2. Hydrogen cycling studies of $CaZn_{11}$ at 580 °C showed sufficient cycling capacity with no significant sintering occurring during heating, as confirmed by scanning electron microscopy, demonstrating its great potential as a TES material for CSP applications. Finally, a cost comparison study of known destabilized CaH_2 systems was carried out to assess the commercial potential.

Introduction

The primary objective of the next-generation concentrating solar power plants (CSP) is to provide continuous electrical power supply at a 40% cost reduction in comparison to the plants currently operating.[1] This cost reduction can be met due to the higher power cycle efficiency achieved in a 600 – 800 °C temperature range by replacing a conventional steam power engine with a Stirling engine.[2] Specifically, the US Department of Energy released the Sun Shot research programme with a target to develop thermal energy storage (TES) materials that operate above 600 °C, have ≥ 95% exergetic efficiency and cost less than \$15/kWh$_{th}$ by 2030. Hence, the identification of a cost-effective high-temperature TES material that meets these requirements is both essential and challenging.[3-7]

There are a plethora of known TES materials that can be categorized depending on their heat storage mechanism, storage density and operating temperature. Sensible heat storage materials, such as molten salts, are the most commonly used TES materials in the industry.[3] Nevertheless, molten salts suffer from several drawbacks such as low energy density (0.02 - 0.03 kWh/kg), corrosion and limited operating temperature (< 565 °C).[8-9] Latent heat storage materials have a higher energy density (0.05 - 0.1 kWh/kg) than the sensible heat storage materials, but most of the materials presently studied have issues such as low thermal conductivity, and high thermal losses.[4, 10-11] To overcome these drawbacks, a third category of TES materials known as thermochemical energy storage is gaining increasing popularity due the high energy density (0.5 – 1 kWh/kg) that these materials possess despite their increased complexity. The superior energy storage properties are based on reversible chemical reactions that take place at high temperatures.[12-13] At present, six systems, namely hydrides, carbonates, hydroxides, oxides, ammonia and organic are identified as thermochemical TES materials.[11] The unique property of metal hydrides to absorb and release hydrogen at a specific pressure at high temperatures, makes them the most promising thermochemical system amongst the rest, and thereby meeting the requirements of the next generation CSP

[a] *Physics and Astronomy, Fuels and Energy Technology Institute, Curtin University, GPO Box U1987, Perth, WA 6845, Australia. E-mail: mark.paskevicius@gmail.com*
[b] *University College Dublin, School of Chemical and Bioprocess Engineering, Belfield, Dublin 4, Ireland, E-mail: veronica.sofianos@ucd.ie*

†Electronic Supplementary Information (ESI) available: Theoretical predictions of possible reaction between CaH_2 and Zn and corresponding H_2 wt. %, vapor pressure curves for pure Ca and Zn and calcium zinc alloys as a function of temperature, Rietveld refinement of the diffraction pattern for the as prepared CaH_2-3Zn. Equilibrium pressure curves of PCI measurements performed at (a) 614 °C (b) 600 °C (c) 580 °C and (d) 565 °C with 3 h desorption step sizes. SEM micrographs of the CaH_2-3Zn after 10 cycles using backscattered electrons and their corresponding EDS spectra.
See DOI: 10.1039/x0xx00000x

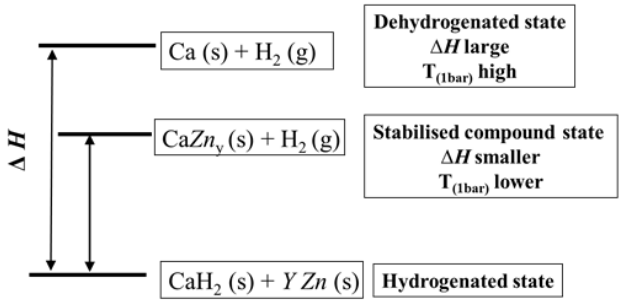

Fig. 1 General enthalpy diagram showing destabilization of CaH_2 by adding Zn through the formation of calcium zinc alloys.[24]

plants.[10, 14-16] Calcium hydride is a promising high-temperature metal hydride due to its: (i) low cost ($6000/ton) and abundance, (ii) low operating hydrogen pressure at high temperature (1 – 5 bar at 1100 – 1400 °C), (iii) high enthalpy of dehydrogenation (207.9 kJmol^{-1} H_2), and (iv) high gravimetric (4939 kJ/kg) and volumetric energy densities (8396 MJ/m^3).[2, 17-18] Its high operating temperature (1100 °C), melting point of both CaH_2 and Ca metal are 816 °C and 842 °C, and expensive tank material requirements to store the corrosive CaH_2, are the main factors that limit the use of pure CaH_2 as a thermochemical TES material.[17, 20-21] Thermodynamic destabilization of CaH_2 using suitable additives, is one approach for reducing the decomposition temperature of CaH_2, and transforming it as a suitable TES material for the third generation CSP plants.[22]

The main novelty of this study lies in the selection of a relatively inexpensive and abundant metal such as zinc ($1.93/kg), to be used as an additive in order to reduce the decomposition temperature of CaH_2 as illustrated in Fig. 1. This method successfully showed by adding Al_2O_3 to CaH_2, where the enthalpy of the reaction was found to be ΔH =100 kJ mol^{-1} H_2 at 636 °C and 1 bar of H_2 pressure.[23] CaH_2-3Zn is an alternate system that exploits the feasibility of Zn as a high-temperature thermochemical TES material for the third generation CSP plants. The aim of this study focused on thermal analysis, and thermodynamic characterization of the CaH_2-3Zn system using mass spectrometry, temperature programmed desorption and *in-situ* X-ray diffraction studies. Its cycling capacity, sample morphology before and after cycling using field emission scanning electron microscopy (FE-SEM) and cost analysis were also investigated and reported.

Experimental Methods

Sample preparation

All chemicals were stored and handled inside an Ar filled MBraun unilab glovebox to reduce oxygen (< 1 ppm) and water (< 1 ppm) contamination. CaH_2 (Sigma Aldrich, > 95% purity powder) and Zn (Chem supply, > 98% purity powder) were mixed in a 1:3 molar ratio and milled under an Ar atmosphere using an Across International Planetary Ball Mill (PQ-N04), employing stainless steel vials and balls. The mixture was ball milled for 3 hours with a 40:1 ball (equal number of 10mm and 6mm diameter balls) to powder ratio. The rotational speed was set to 400 rpm with a change of direction every 30 minutes without pausing.

Sample Characterization

Theoretical Predictions

The possible reaction pathways between CaH_2 and Zn were predicted using the phase diagram of the Ca-Zn system.[25-26] The volatility of solid calcium zinc alloys are linked with the vapor pressure of Zn. The vapor pressure of pure Zn metal and Ca was calculated from room temperature to 1000 °C.[27] Vapor pressure data of calcium zinc solid alloys were also derived from Chiotti *et al.* [37]and Hodge *et al*. [39] and the vapor pressures of eight calcium zinc alloys (Ca_3Zn, Ca_5Zn_3, CaZn, $CaZn_2$, $CaZn_3$, $CaZn_5$, $CaZn_{11}$ and $CaZn_{13}$) were plotted along with pure Zn and Ca as a function of temperature in Figure S1. Among the eight solid alloys, Zn rich alloys have high vapor pressures and are less volatile than Zn poor alloys at higher temperatures (> 600 °C).

Powder X-ray Diffraction

Ex-situ powder X-ray diffraction (XRD) was used to identify the crystalline materials in each sample. Airtight polymethyl methacrylate domed sample holders were used to avoid oxygen and moisture contamination during data collection. Data were collected using a Bruker D8 Advance Diffractometer with a copper X-ray tube (λ = 1.5418 Å, 40 kV, 40 mA) in the 10° – 80° 2ϑ range with a 0.03° step size and 1.6 s/step count time. The diffraction peaks were quantitatively analyzed by the Rietveld method[28] using the Bruker TOPAS Version 5 software.[29] The structural information was extracted from ICDD PDF4 database and the Crystallography Open Database (COD).[30]

In-situ X-ray diffraction was performed using a Thermo Fisher ARL Equinox 5000 diffractometer (λ = 0.7093 Å, Mo-Kα, 50 kV, 30 mA). The sample was loaded into a quartz capillary tube (0.7 mm outer diameter, 0.01 mm wall thickness), sealed and then mounted onto a sample holder inside an Ar filled glovebox. The sample was heated from room temperature to 692 °C using a hot air blower (5 °C/min) and kept isothermal for 2 hours. Data were acquired on a CPS 120 detector (0 - 60° 2ϑ) with a 60 s exposure time. The temperature of the hot air blower was calibrated against the known thermal expansion coefficient of both NaCl and Ag.[31-33]

Mass Spectrometry

Temperature programmed desorption-mass spectrometry (TPD-MS) measurements were obtained using a Stanford Research Systems (SRS, RGA-300) residual gas analyzer consisting of a quadrupole mass spectrometer.[34] A 3 mg sample of pure CaH_2 and CaH_2-3Zn was placed in a stainless steel sample holder inside a silicon carbide reactor that was connected to the spectrometer. The samples were heated to 850 °C at 5 °C/min under high vacuum (< 7 x 10^{-4} mbar). The corresponding analogue scan of partial pressure *vs* mass to charge ratio was obtained from the RGA software. A K-type

thermocouple with an uncertainty of ± 1.5 °C was connected inside the SiC tube to record the temperature of the sample.

Temperature Programmed Desorption and Pressure Composition Isotherms

H_2 sorption properties were studied by Temperature Programmed Desorption (TPD), using a computer-controlled Sievert's apparatus.[35] CaH_2-3Zn was heated to either 630 °C or 830 °C, with 5 °C/min heating rates. The powder mixture was placed inside a stainless-steel sample holder and then loaded into a silicon carbide (SiC) reactor. H_2 has a negligible hydrogen permeation through SiC at high temperatures (> 450 °C) and therefore was chosen as the most suitable reactor material for such measurements.[35-36] The sample temperature was measured using a K-type thermocouple which is kept inside the SiC reactor and direct contact with the sample. Pressure Composition Isotherm (PCI) measurements of CaH_2-3Zn were conducted on the same apparatus to acquire the thermodynamic properties of the dehydrogenation reaction between 565 °C and 614 °C with a 1 bar pressure step size and a 3 h equilibration time per step. H_2 desorption and absorption cycling studies were performed on CaH_2-3Zn at 580 °C with a ramp rate of 5 °C/min. The H_2 pressure and equilibration time during desorption was ~ 0.8 bar and 3 h respectively, whereas during absorption it was ~2.8 bar and 5 h.

Scanning Electron Microscopy and Energy Dispersive X-ray Spectroscopy

Field emission scanning electron microscopy (FE-SEM) and energy dispersive X-ray spectroscopy were carried out using a Tescan Mira3 integrated with EBSD/EDS Oxford Instrument detectors controlled by the Aztec software. The SEM images of the CaH_2-3Zn system before and after cycling were collected using both secondary and back-scattered electron detectors. The SEM samples were prepared inside an Ar filled glove box by placing a small amount of powder onto a carbon tape, and then transferred to the SEM chamber with minimum air exposure.

Results and Discussion

Theoretical Predictions

The phase diagram of the Ca-Zn system shows eight different alloys (Ca_3Zn, Ca_5Zn_3, CaZn, $CaZn_2$, $CaZn_3$, $CaZn_5$, $CaZn_{11}$ and $CaZn_{13}$) at different molar ratios.[25-26] Table S1 indicates theoretically possible reactions between CaH_2 and Zn and the corresponding theoretical H_2 wt%. The vapor pressure of Zn plays a vital role in the formation and volatility of the solid alloy formation.[27, 37-39] Fig. S1 shows the vapor pressure curve of pure Ca, Zn and solid calcium zinc alloys as a function of temperature. It shows that the vapor pressure of pure Zn is higher than pure Ca until 600 °C, after which the vapor pressure of Zn is less than that of pure Ca. From Fig. S1 and the Ca-Zn phase diagram it can be seen that Zn rich alloys have higher vapor pressures and hence are less likely to produce vaporized Zn above 600 °C.[25] Moreover, above ~ 700 °C no calcium zinc solid alloys exist.

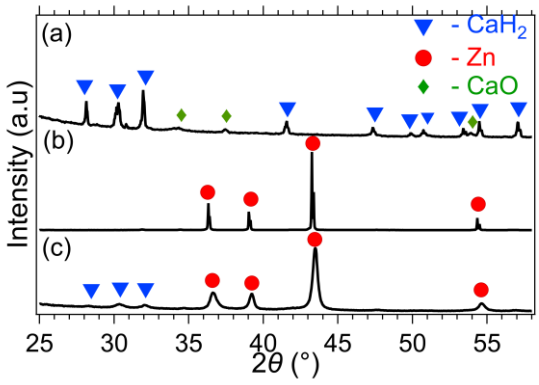

Fig. 2 *Ex-situ* XRD patterns of (a) CaH_2, (b) Zn and (c) CaH_2-3Zn system after ball milling using Cu K_α radiation (λ = 1.5418 Å).

Initial Phase Analysis

The diffraction patterns of as-supplied CaH_2, Zn and ball-milled CaH_2-3Zn are presented in Fig. 2 a, b and c, respectively. Quantitative phase analysis was used to determine the purity of the materials using the Rietveld method. Quantitative phase analysis of the CaH_2 reagent shows CaH_2 with a negligible amount of crystalline CaO, while the XRD and refinement pattern for the ball milled CaH_2-3Zn only shows CaH_2 (16.5 ± 0.8 wt%), and Zn (83 ± 1 wt%) (Fig. 2 c and Fig. S2). This indicates that no reaction occurred between CaH_2 and Zn during ball milling to form a Ca-Zn product as expected by the high required enthalpy of reaction.

The Destabilization of CaH_2 Using Zn

TPD-MS measurements were performed on CaH_2 and CaH_2-3Zn to compare the H_2 gas release profiles as a function of temperature (Fig. 3 a and b respectively). Due to the high vacuum (< 7 x 10^{-4} mbar) employed in this technique, CaH_2 commenced H_2 release at 500 °C and reached the highest rate of hydrogen release at 600 °C (Fig. 3 a), with the single decomposition peak indicative of a one-step decomposition reaction. The H_2 desorption profile of CaH_2-3Zn (Fig. 3 b) consisted of three H_2 peaks denoting a three-step decomposition reaction, either due to differing kinetics or thermodynamics of reaction. The first small peak appeared at

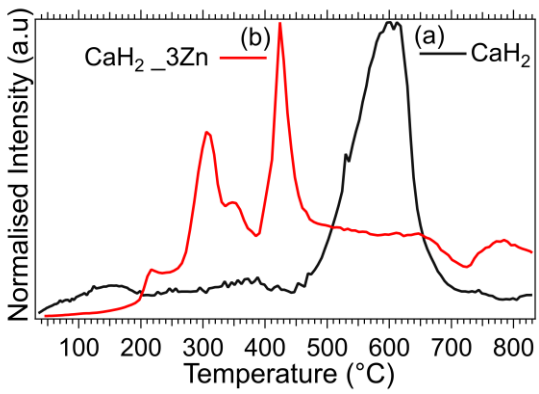

Fig. 3 H_2 desorption profiles as observed by TPD-MS measurements of (a) CaH_2 and (b) CaH_2-3Zn while heating under vacuum.

200 °C, followed by two high intensity peaks at 300 °C and 420 °C, respectively. H_2 was the only gas detected during heating to 800 °C. The three low-temperature decomposition peaks of the CaH_2-3Zn sample show that the addition of Zn thermodynamically destabilizes the CaH_2.

Thermal Analysis

A TPD measurement was conducted on CaH_2-3Zn by heating the sample from room temperature to 830 °C (5 °C/min), before keeping the temperature isothermal at 830°C for 10 hours to check the volatility of the alloy formed (Fig. 4 a). The measurement was commenced under initial static vacuum and reached a maximum H_2 pressure of 0.9 bar. After 2 hours at 830 °C the hydrogen pressure began to decrease. The reason for this pressure decrease was due to: (i) zinc evaporation from the alloy as evidenced by zinc metal deposition on the cool regions of the sample cell, and (ii) H_2 reabsorption into the zinc-poor calcium metal to reform CaH_2. This was confirmed from the sample's *ex-situ* XRD pattern obtained after the TPD measurement (Fig. 5 a), which comprised of CaH_2 and Zn peaks with no calcium zinc alloy peaks being present. The TPD measurement was repeated with a maximum temperature of 630 °C and a subsequent isotherm for 10 h. A maximum H_2 pressure of 0.58 bar was reached starting from vacuum. Fig. 4 b illustrates the TPD profile, which exhibits an almost isobaric profile after reaching 630 °C with reduced Zn evaporation

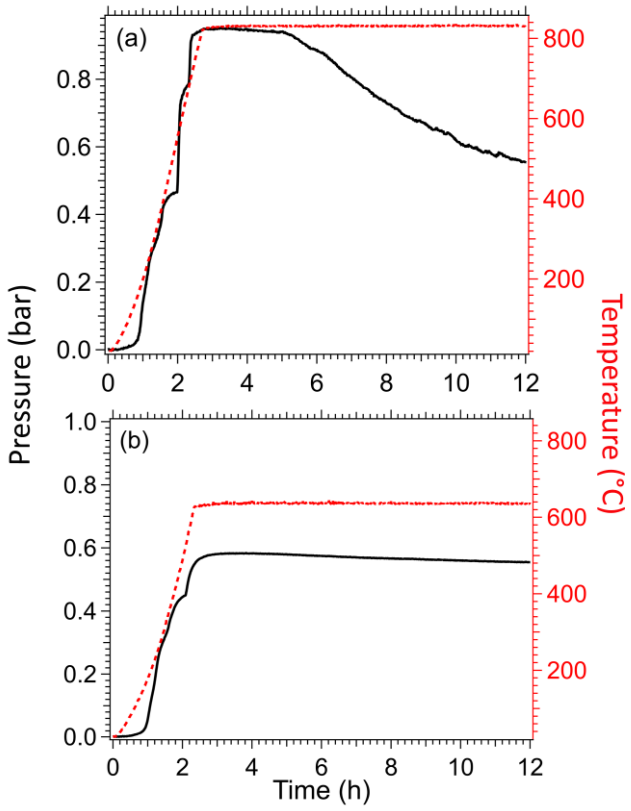

Fig. 4 TPD profiles of CaH_2-3Zn from room temperature to (a) 830 °C and (b) 630 °C. Black solid line = pressure, red dotted line = temperature.

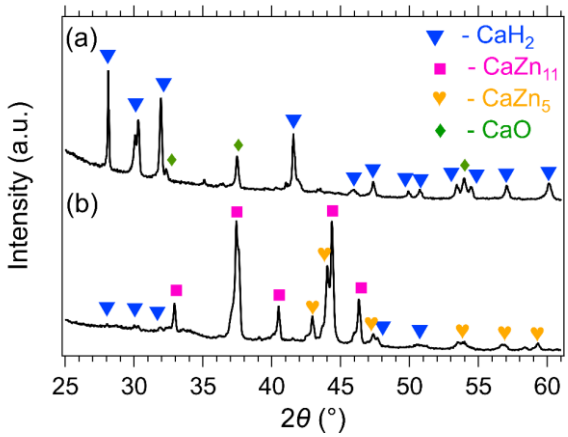

Fig. 5 *Ex-situ* XRD pattern of CaH_2-3Zn after the TPD measurements at (a) 830 °C and (b) 630 °C (Cu Kα, λ = 1.5418 Å).

observed in comparison to the data obtained at 830 °C. $CaZn_{11}$ and $CaZn_5$ alloys were the main decomposition products at 630 °C as confirmed by the sample's *ex-situ* XRD pattern obtained after the TPD measurement (Fig. 5 b).

Identifying the Reaction Pathway by *in-situ* X-ray Diffraction

In-situ XRD data of CaH_2-3Zn during thermal ramping under argon is presented in Fig. 6 a and is compared with its differential TPD profile (Fig. 6 b). It is evident from the *in-situ* XRD patterns that the reaction between CaH_2 and Zn occurs in a three-step reaction between 190 and 590 °C, which is in a good agreement with the TPD profiles. It is clear from Fig. 6 a the three different alloys formed are $CaZn_{13}$, $CaZn_{11}$ and $CaZn_5$ at three different temperature ranges of 190 – 390 °C, 390 – 590 °C and > 590 °C, respectively. The experimental reaction can be predicted from the *in-situ* XRD data as follows, which shows the presence of excess CaH_2.

$$CaH_2 + 3Zn \rightarrow \frac{3}{13}CaZn_{13} + \frac{10}{13}CaH_2 + \frac{3}{13}H_{2\,(g)} \quad (1)$$

$$\frac{3}{13}CaZn_{13} + \frac{10}{13}CaH_2 \rightarrow \frac{3}{11}CaZn_{11} + \frac{8}{11}CaH_2 + \frac{6}{143}H_{2\,(g)} \quad (2)$$

$$\frac{3}{11}CaZn_{11} + \frac{8}{11}CaH_2 \rightarrow \frac{3}{5}CaZn_5 + \frac{2}{5}CaH_2 + \frac{18}{55}H_{2\,(g)} \quad (3)$$

Thermodynamic Calculations

As the *ex-situ* XRD pattern of CaH_2-3Zn after the TPD measurement at 830 °C did not exhibit any solid calcium-zinc alloy present in the decomposed sample, PCI measurements were performed at temperatures below 630 °C. The measurements were carried out at 565, 580, 600 and 614 °C (Fig. 7 a). The corresponding van't Hoff plot (Fig. 7 b) was constructed by plotting the midpoint values from the first plateau region of each PCI measurement to acquire the enthalpy and entropy of reaction. The optimized form (no excess CaH_2) of the above mentioned three reactions can be written as follows:

$$CaH_2 + 13Zn \rightarrow CaZn_{13} + H_{2\,(g)} \quad (4)$$

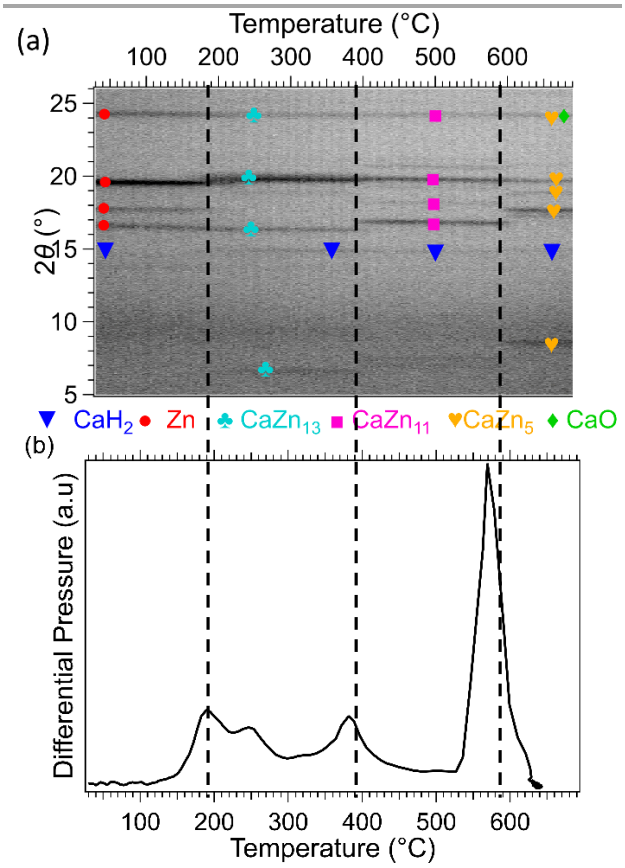

Fig. 6 (a) *In-situ* XRD patterns of CaH_2–3Zn from room temperature to 690 °C (Mo Kα of λ = 0.7093 Å). (b) Differential TPD profiles of CaH_2-3Zn from room temperature to 640 °C.

$$CaH_2 + 11Zn \rightarrow CaZn_{11} + H_{2\,(g)} \quad (5)$$

$$CaH_2 + \tfrac{5}{6}CaZn_{11} \rightarrow \tfrac{11}{6}CaZn_5 + H_{2\,(g)} \quad (6)$$

The corresponding enthalpy and entropy of the optimized reaction (5), obtained from first plateau as shown in Figure a, were calculated as ΔH_{des} = 131.5 ± 4.0 kJ.mol^{-1} H_2, ΔS_{des} = 151.1 ± 4.0 J.K^{-1}.mol^{-1} H_2, respectively. Therefore, the equilibrium desorption temperature at 1 bar pressure is $T_{des} = \Delta H/\Delta S$ = 597 ± 35 °C. The pressure curves of each PCI measurement show that thermodynamic equilibrium was reached for each of the 3 h desorption steps, indicating fast reaction kinetics (Fig. S3). The existence of two plateau regions in the PCI measurements is evident from Fig. 7 a. The second plateau region is not accurately measured due to (i) zinc evaporation (rate is high at higher temperatures and also depends on time exposed at that temperature) and (ii) limitation of the Sievert's apparatus to achieve very low pressure increments (< 1mbar). The formation of $CaZn_{11}$ from reaction (5) followed by $CaZn_5$ from reaction (6) during the PCI measurements were confirmed using e*x-situ* XRD. Fig. 8 a and b show the XRD patterns of CaH_2-3Zn confirmed $CaZn_{11}$ to be the main phase with only minor $CaZn_5$ peaks present, whereas Fig. 8 b shows that all $CaZn_{11}$ peaks have been replaced with $CaZn_5$ peaks formed during the second equilibrium pressure region. These XRD findings confirm the reactions given above (4 - 6).

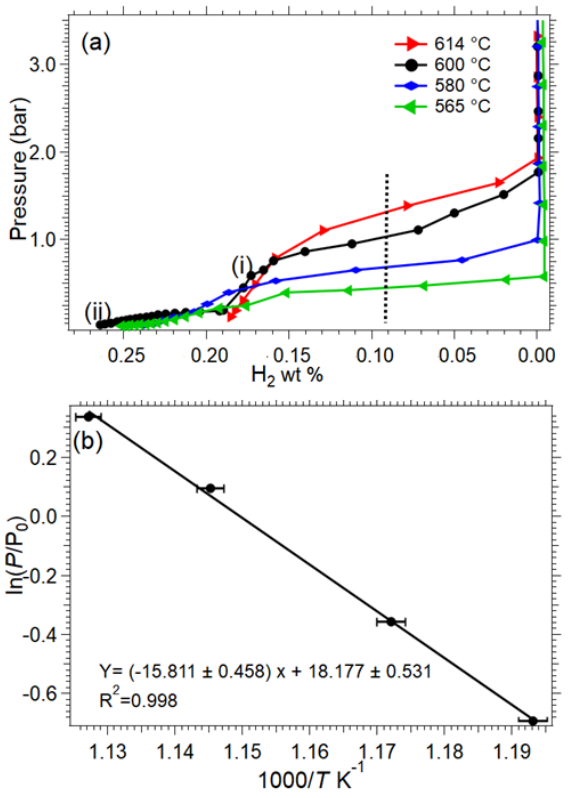

Fig. 7 (a) Pressure Composition Isotherms of CaH_2-3Zn between 565 °C (green), 580 °C (blue), 600 °C (black) and 614 °C (red) and (b) the corresponding van't Hoff plot.

Cycling Studies

CaH_2-3Zn was cycled at 580 °C, which follows the proposed optimized reaction expressed in eq. (5), to assess its H_2 cycling capacity and thermochemical reversibility. This temperature was chosen in order to reduce the Zn evaporation rate from the sample. Fig. 9 illustrates the ten H_2 desorption and absorption cycles showing good thermochemical reversibility overall. Each desorption and absorption step was 3 and 5 hrs, respectively. It is evident from Fig. 9 that the kinetics of the desorption reaction are faster than absorption. However, none of the reactions were completed within the allocated step time. The evaporation of Zn from the formed

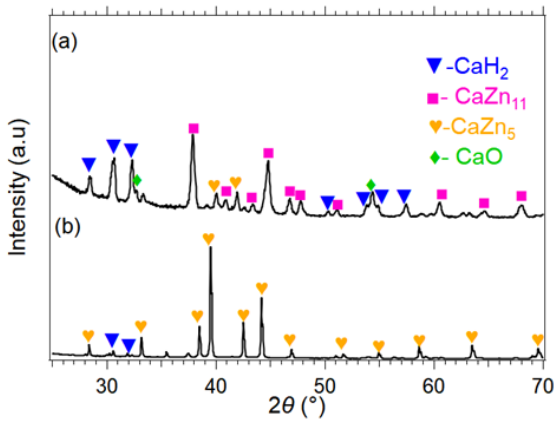

Fig. 8 *Ex-situ* XRD patterns of CaH_2-3Zn in the marked regions (a) at (i) and (b) at (ii) in the Fig. 7(a) from the PCI measurement at 600 °C (Cu K_α, λ = 1.5418 Å).

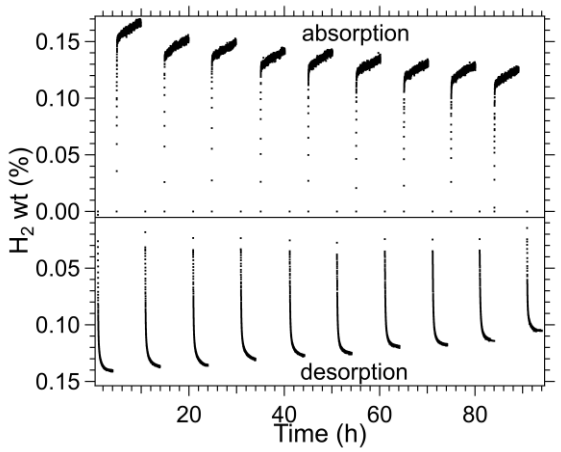

Fig. 9 H_2 desorption and absorption cycles of the CaH_2-3Zn mixture at 580 °C.

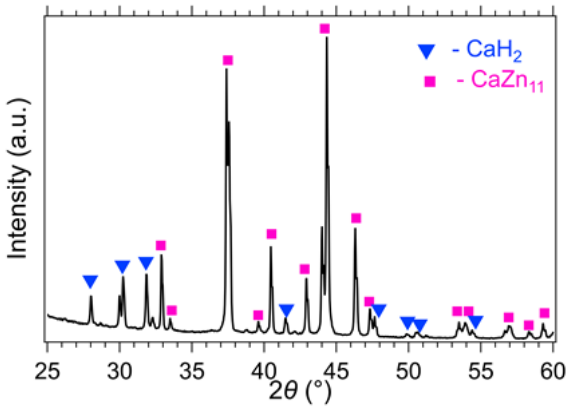

Fig. 10 *Ex-situ* XRD pattern of the CaH_2-3Zn mixture as prepared after cycling at 580 °C (Cu Kα, λ = 1.5418 Å).

calcium zinc alloy during cycling was also confirmed from the presence of Zn metal deposition on the colder regions of the reactor. Therefore, after the completion of the 10th cycle, 80 % of its initial capacity was retained. The cycling capacity of CaH_2-3Zn may be enhanced by improving the design of the sample holder so that it can contain the evaporated Zn and also by initially synthesizing with 1:11 molar ratio of CaH_2: Zn. This may result in a complete desorption and absorption reaction upon cycling within the allocated waiting times.

Also, it may allow more cycles without degradation as commercial thermochemical storage system requires a cycling reliability of up to 10000 cycles over a 30 year lifespan for CSP plants. An *ex-situ* XRD pattern (Figure 10) was obtained after the 10th desorption cycle, confirming that $CaZn_{11}$ was the main crystalline phase present in the decomposed samples, as previously confirmed from TPD, PCT and *in-situ* XRD studies.

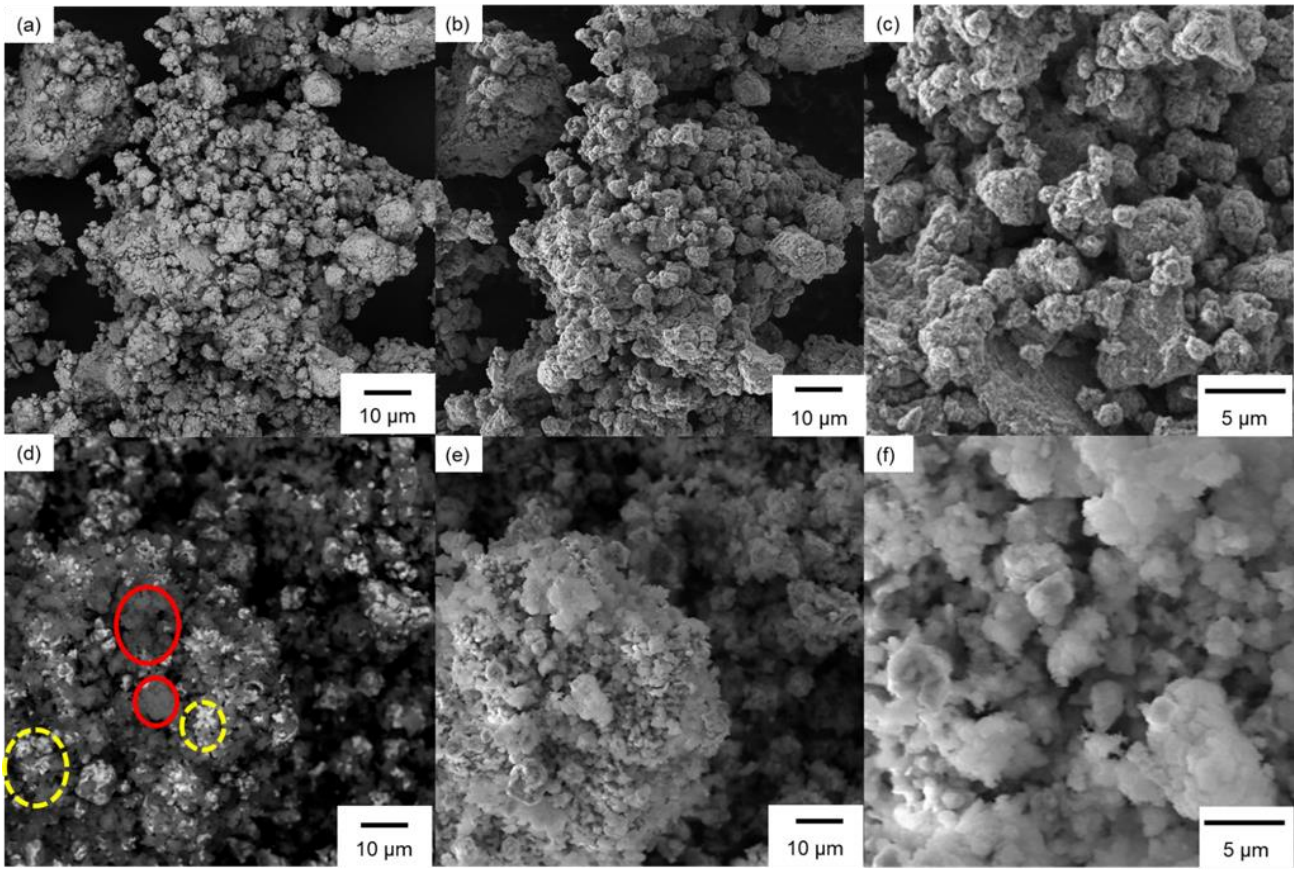

Fig. 11 SEM micrographs of the CaH_2-3Zn mixture using (a) back scattered electrons, (b, c) secondary electrons before cycling, and (d) back scattered and (e, f) secondary electrons after 10 cycles at 580 °C.

Morphological Studies

SEM micrographs of CaH_2-3Zn before and after cycling are presented in Fig. 11 a - c and Fig. 11 d - f, respectively. It is evident from Fig. 11 a, obtained using backscattered electrons, that CaH_2 and Zn are evenly distributed through the sample creating a homogenous powder after ball-milling. No distinctive bright and dark areas were observed in the micrograph that may have been created due to areas with inhomogeneous distributions of particles with excessively different atomic number, as observed in Fig. 11 d after cycling is performed. Specifically, the bright areas in Fig. 11 d indicated with yellow dashed circles are areas rich in Zn, whereas the dark areas indicated with red circles are Ca rich, as confirmed by their associated EDS spectra (Fig. S4). To study the morphological differences before and after cycling, Fig. 11 b, c and 11 e, f were obtained using secondary electrons. It can be seen from Fig. 11 c and f that the powder particles before and after cycling are relatively the same size and the particles did not sinter or melt upon heating, as often is the case with other metal hydrides at temperatures above 500 °C.[2]

Cost

A cost comparison of the present system with other destabilized CaH_2 systems and molten salt is listed in Table 1. The cost of the raw material (CaH_2-11Zn) is currently estimated as \$55/ $kWh_{th,}$[19, 40] which is higher than molten salts and other destabilized CaH_2 systems, such as Al and Al_2O_3 while significantly less compared with $LiBH_4$ as shown in Table 1.[43-44] However, the CaH_2-11Zn system possesses high enthalpy of reaction and relatively low operating pressure at the working temperature (1 bar H_2 pressure at~ 600 °C) compared with the CaH_2-Al system (62 bar H_2 pressure at~ 700 °C).[2,41] Overall the high cost, multistep reactions and Zn evaporation issues makes the CaH_2-3Zn system challenging to use as a commercial thermochemical storage material.

Table 1. Cost Comparison Study of CaH_2-3Zn System with Pure CaH_2, other CaH_2 Destabilized Systems and Molten Salt in the CSP Scenario*.

TES Material	ΔH kJ.mol^{-1} H_2	ΔH kJ/kg	US \$/ ton	US \$/ kWh-thermal	T (°C)	P (bar)	Mass required tonnes+	Ref.
CaH_2	207.9	4939	6000	4.4	1000	1.2	265	2,19
CaH2 + 11Zn	131	172	2649	55.4	597	1	8920	40
$3CaH_2 + 2Al_2O_3$	100	909	2460	9.7	636	1	1650	23
$CaH_2 + 2Al$	84	874	3631	14.9	700	62	1660	2, 23,41-42
$CaH_2 + 6LiBH_4$	60	347	190500	1976	450	10	4960	43-44
Molten salt (40 $NaNO_3$: 60 KNO_3)	39	413	630	5.8	565	–	5250	19

*Note that values were calculated in an assumption of 100 % conversion of reactants.

+ To generate 1TJ of energy

Conclusions

This study has developed a novel approach to thermodynamically destabilize CaH_2 by adding low cost Zn metal in a 1:3 molar ratio, and investigate its potential as a TES material for third generation CSP plants. *In-situ* XRD diffraction studies showed the formation of three different calcium zinc alloys, $CaZn_{13}$, $CaZn_{11}$ and $CaZn_5$, at 190, 390 and 590 °C, respectively. The enthalpy and entropy of formation of CaH_2-3Zn system was found to be ΔH_{des} = 131 ± 4 kJ.mol^{-1} H_2, ΔS_{des} = 151 ± 4 J.K^{-1}.mol^{-1} H_2, respectively. The CaH_2-3Zn system's operating condition was found to be 597 ± 35 °C at 1 bar of H_2 pressure. Cycling studies of the material over the first step of the reaction show reasonable thermochemical reversibility over 10 cycles. SEM studies before and after cycling confirmed no significant sintering of the sample upon heating. The cost of the raw material was estimated as \$55/kWh_{th}. The destabilization of CaH_2 with Zn proves that thermodynamic destabilization can be achieved, but lower cost destabilizing agents must be found. It is challenging to predict the optimal reaction pathways for these destabilization reactions due to unreliable thermodynamic predictions for several reaction products.

Conflicts of interest

There are no conflicts to declare.

Acknowledgements

C.E.B., M.P., T.D.H. and M.V.S. acknowledge the financial support of the Global Innovation Linkage (GIL73589). C.E.B. acknowledges the financial support of ARC Linkage grant LP150100730, and ARC LIEF grants LE0775551 and LE0989180, which enabled the TPD and PCI measurements to be undertaken. M.V.S. acknowledges the financial support of the UCD Ad Astra Fellowship, M.P. acknowledges the financial support of the Australian Research Council (ARC) Future Fellowship (FT160100303). C.E.B. acknowledge the financial support of the ARC for the ARC LIEF grant LE170100199, which

enabled the in-situ XRD measurements. The authors acknowledge the technical assistance of Matthew Rowles and the facilities of the Microscopy & Microanalysis Facility of the John de Laeter Centre at Curtin University.

References

1 Murphy, C.; Sun, Y.; Cole, W. J.; Maclaurin, G. J.; Mehos, M. S.; Turchi, C. S. The Potential Role of Concentrating Solar Power within the Context of DoE's 2030 Solar Cost Targets; National Renewable Energy Lab. NREL/TP-6A20-7191, 2019.

2 Manickam, K.; Mistry, P.; Walker, G.; Grant, D.; Buckley, C. E.; Humphries, T. D.; Paskevicius, M.; Jensen, T.; Albert, R.; Peinecke, K., Future Perspectives of Thermal Energy Storage with Metal Hydrides. *International Journal of Hydrogen Energy* 2019, **44**, 7738-7745.

3 Pelay, U.; Luo, L.; Fan, Y.; Stitou, D.; Rood, M., Thermal Energy Storage Systems for Concentrated Solar Power Plants. *Renewable and Sustainable Energy Reviews* 2017, **79**, 82-100.

4 Chen, X.; Zhang, Z.; Qi, C.; Ling, X.; Peng, H., State of the Art on the High-Temperature Thermochemical Energy Storage Systems. *Energy conversion and management* 2018, **177**, 792-815.

5 Carrillo, A. J.; González-Aguilar, J.; Romero, M.; Coronado, J. M., Solar Energy on Demand: A Review on High Temperature Thermochemical Heat Storage Systems and Materials. *Chemical reviews* 2019, **119**, 4777-4816.

6 US Department of Energy, D.O.E. Sunshot Vision Study. (accessed Jun 02, 2020).

7 The Potential Role of Concentrating Solar Power within the Context of Doe's 2030 Solar Cost Targets (accessed Jun, 2020)

8 Ho, C. K., A Review of High-Temperature Particle Receivers for Concentrating Solar Power. *Applied Thermal Engineering* 2016, **109**, 958-969.

9 Valverde, J. M.; Barea-Lopez, M.; Perejon, A.; Sanchez-Jimenez, P. E.; Perez-Maqueda, L. A., Effect of Thermal Pretreatment and Nanosilica Addition on Limestone Performance at Calcium-Looping Conditions for Thermochemical Energy Storage of Concentrated Solar Power. *Energy & Fuels* 2017, **31**, 4226-4236.

10 Harries, D. N.; Paskevicius, M.; Sheppard, D. A.; Price, T. E. C.; Buckley, C. E., Concentrating Solar Thermal Heat Storage Using Metal Hydrides. *Proceedings of the IEEE* 2011, **100**, 539-549.

11 Pardo, P.; Deydier, A.; Anxionnaz-Minvielle, Z.; Rougé, S.; Cabassud, M.; Cognet, P., A Review on High Temperature Thermochemical Heat Energy Storage. *Renewable and Sustainable Energy Reviews* 2014, **32**, 591-610.

12 Ervin, G., Solar Heat Storage Using Chemical Reactions. *Journal of solid state chemistry* 1977, **22**, 51-61.

13 Gil, A.; Medrano, M.; Martorell, I.; Lázaro, A.; Dolado, P.; Zalba, B.; Cabeza, L. F., State of the Art on High Temperature Thermal Energy Storage for Power Generation. Part 1—Concepts, Materials and Modellization. *Renewable and Sustainable Energy Reviews* 2010, **14**, 31-55.

14 Lai, Q.; Paskevicius, M.; Sheppard, D. A.; Buckley, C. E.; Thornton, A. W.; Hill, M. R.; Gu, Q.; Mao, J.; Huang, Z.; Liu, H. K., Hydrogen Storage Materials for Mobile and Stationary Applications: Current State of the Art. *ChemSusChem* 2015, **8**, 2789-2825.

15 Sheppard, D.; Corgnale, C.; Hardy, B.; Motyka, T.; Zidan, R.; Paskevicius, M.; Buckley, C., Hydriding Characteristics of $NaMgH_2$ F with Preliminary Technical and Cost Evaluation of Magnesium-Based Metal Hydride Materials for Concentrating Solar Power Thermal Storage. *RSC Advances* 2014, **4**, 26552-26562.

16 M. Hirscher, V. A. Yartys, M. Baricco, J. B. von Colbe, D. Blanchard, R. C. Bowman, D. P. Broom, C. E. Buckley, F. Chang, P. Chen, Y. W. Cho, J. C. Crivello, F. Cuevas, W. I. F. David, P. E. de Jongh, R. V. Denys, M. Dornheim, M. Felderhoff, Y. Filinchuk, G. E. Froudakis, D. M. Grant, E. M. Gray, B. C. Hauback, T. He, T. D. Humphries, T. R. Jensen, S. Kim, Y. Kojima, M. Latroche, H. W. Li, M. V. Lototskyy, J. W. Makepeace, K. T. Moller, L. Naheed, P. Ngene, D. Noreus, M. M. Nygard, S. I. Orimo, M. Paskevicius, L. Pasquini, D. B. Ravnsbaek, M. V. Sofianos, T. J. Udovic, T. Vegge, G. S. Walker, C. J. Webb, C. Weidenthaler and C. Zlotea, Journal of Alloys and Compounds, 2020, **827**, 153548.

17 Rönnebro, E. C.; Whyatt, G.; Powell, M.; Westman, M.; Zheng, F. R.; Fang, Z. Z., Metal Hydrides for High-Temperature Power Generation. *Energies* 2015, **8**, 8406-8430.

18 Sheppard, D.; Paskevicius, M.; Humphries, T.; Felderhoff, M.; Capurso, G.; von Colbe, J. B.; Dornheim, M.; Klassen, T.; Ward, P.; Teprovich, J., Metal Hydrides for Concentrating Solar Thermal Power Energy Storage. *Applied Physics A* 2016, **122**, 395.

19 Humphries, T. D.; Møller, K. T.; Rickard, W. D.; Sofianos, M. V.; Liu, S.; Buckley, C. E.; Paskevicius, M., Dolomite: A Low Cost Thermochemical Energy Storage Material. *Journal of Materials Chemistry A* 2019, **7**, 1206-1215.

20 Curtis, R.; Chiotti, P., Thermodynamic Properties of Calcium Hydride1. *The Journal of Physical Chemistry* 1963, **67**, 1061-1065.

21 Peterson, D.; Fattore, V., Calcium-Calcium Hydride Phase System1. *The Journal of Physical Chemistry* 1961, **65**, 2062-2064.

22 Sofianos, M. V.; Randall, S.; Paskevicius, M.; Aguey-Zinsou, K.-F.; Rowles, M. R.; Humphries, T. D.; Buckley, C. E., Exploring Halide Destabilised Calcium Hydride as a High-Temperature Thermal Battery. *Journal of Alloys and Compounds* 2020, **819**, 153340.

23 Balakrishnan, s.; Sofianos, M. V.; Paskevicius, M.; Rowles, M. R.; Buckley, C. E., Destabilised Calcium Hydride as a Promising High-Temperature Thermal Battery. *The Journal of Physical Chemistry C* 2020.

24 Vajo, J. J.; Olson, G. L., Hydrogen Storage in Destabilized Chemical Systems. *Scripta Materialia* 2007, **56**, 829-834.

25 Okamoto, H., Ca-Zn (Calcium-Zinc). *Journal of Phase Equilibria and Diffusion* 2013, **34**, 171-171.

26 Messing, A.; Adams, M.; Steunenberg, R. *Contribution to the Phase Diagram Calcium-Zinc*; Argonne National Lab., Ill.: 1962.

27 Vapor Pressure Calculator. https://www.iap.tuwien.ac.at/www/surface/vapor_pressure (accessed May 20, 2020)

28 Rietveld, H., A Profile Refinement Method for Nuclear and Magnetic Structures. *Journal of applied Crystallography* 1969, **2**, 65-71.

29 Coelho, A. A., Topas and Topas-Academic: An Optimization Program Integrating Computer Algebra and Crystallographic Objects Written in C++. *Journal of Applied Crystallography* 2018, **51**, 210-218.

30 Gražulis, S.; Daškevič, A.; Merkys, A.; Chateigner, D.; Lutterotti, L.; Quiros, M.; Serebryanaya, N. R.; Moeck, P.; Downs, R. T.; Le Bail, A., Crystallography Open Database (Cod): An Open-Access Collection of Crystal Structures and Platform for World-Wide Collaboration. *Nucleic acids research* 2011, **40**, D420-D427.

31 Pathak, P.; Vasavada, N., Thermal Expansion of Nacl, Kcl and Csbr by X-Ray Diffraction and the Law of Corresponding States. *Acta Crystallographica Section A: Crystal Physics, Diffraction, Theoretical and General Crystallography* 1970, **26**, 655-658.

32 Hu, J.; Cai, W.; Li, C.; Gan, Y.; Chen, L., In Situ X-Ray Diffraction Study of the Thermal Expansion of Silver Nanoparticles in

Ambient Air and Vacuum. *Applied Physics Letters* 2005, **86**, 151915.

33 Hansen, B. R.; Møller, K. T.; Paskevicius, M.; Dippel, A.-C.; Walter, P.; Webb, C. J.; Pistidda, C.; Bergemann, N.; Dornheim, M.; Klassen, T., In Situ X-Ray Diffraction Environments for High-Pressure Reactions. *Journal of Applied Crystallography* 2015, **48**, 1234-1241.

34 SRS. RGA Windows Software v.3.2. https://Www.Thinksrs.Com/Products/Vac.html (accessed August 18, 2020).

35 Sheppard, D. A.; Paskevicius, M.; Javadian, P.; Davies, I. J.; Buckley, C. E., Methods for Accurate High-Temperature Sieverts-Type Hydrogen Measurements of Metal Hydrides. *Journal of Alloys and Compounds* 2019, **787**, 1225-1237.

36 Alonso, J. A.; Retuerto, M.; Sanchez-Benitez, J.; Fernández-Díaz, M. T., Crystal Structure and Bond Valence of CaH_2 from Neutron Powder Diffraction Data. *Zeitschrift für Kristallographie-Crystalline Materials* 2010, **225**, 225-229.

37 Chiotti, P.; Hecht, R., Thermodynamic Properties of the Calcium-Zinc System. *Transactions of the Metallurgical Society of AIME* 1967, **239**, 536-541.

38 Itkin, V.; Alcock, C., The Ca-Zn (Calcium-Zinc) System. *Bulletin of Alloy Phase Diagrams* 1990, **11**, 328-333.

39 Hodge, W.; Jaffe, R.; Gonser, B. *Calcium and Calcium-Base Alloys*; Battelle Memorial Inst., Columbus, OH, Project MX-791 Contr. W33-038-ac-14105, 1949.

40 Zn Metal Prices. https://markets.businessinsider.com/commodities/zinc-price (Accessed Apr 20, 2020).

41 Ward, P. A.; Teprovich Jr, J. A.; Liu, Y.; He, J.; Zidan, R., High Temperature Thermal Energy Storage in the $CaAl_2$ System. *Journal of Alloys and Compound*s 2018, **735**, 2611-2615.

42 Veleckis, E., Application of the Hydrogen Titration Method to a Thermodynamic Investigation of Solid Al-Ca Alloys. *Journal of the Less Common Metals* 1981, **80**, 241-255.

43 Li, Y.; Li, P.; Qu, X., Investigation on $LiBH_4$-CaH_2 Composite and Its Potential for Thermal Energy Storage. *Scientific reports* 2017, **7**, 41754.

44 $LiBH_4$ Prices. https://www.sigmaaldrich.com/catalog/search?term=LiBH4&interface=All&N=0&mode=partialmax&lang=en&region=AU&focus=product (Accessed Apr 20, 2020).